2. PHYSICAL CHARACTERISTICS OF THE TEST AREA NORTH (WAG 1)

This section describes the physical setting of the Waste Area Group (WAG) 1 study area in terms of physical characteristics of physiography, meteorology, geology, and hydrology. Regional and local characteristics are discussed.

2.1 Physiography

The Snake River Plain (SRP) is the largest continuous physiographic feature in southern Idaho, as shown in Figure 2-1. This large topographic depression extends from the Oregon border across southern Idaho to Yellowstone National Park and northwestern Wyoming.

The SRP slopes upward from an elevation of about 750 m (2,500 ft) at the Oregon border to over 1,500 m (5,000 ft) at Ashton, northeast of the Idaho National Engineering and Environmental Laboratory (INEEL). The SRP is composed of two structurally dissimilar segments, with the division occurring between the towns of Bliss and Twin Falls, Idaho. West of Twin Falls, the Snake River has cut a valley through tertiary basin fill sediments and interbedded volcanic rocks. The stream drainage is well developed, except in a few areas covered by recent thin basalt flows. East of Bliss, Idaho, the complexion of the plain changes as the Snake River locally carves a vertical-walled canyon through thick sequences of Quaternary basalt with few interbedded sedimentary deposits.

The INEEL is located on the northern edge of the Eastern Snake River Plain (ESRP), a 50-to-70-mi-wide northeastern-trending basin extending from the vicinity of Bliss on the southwest to the Yellowstone Plateau on the northeast. Three mountain ranges end at the northern and northwestern boundaries of the INEEL: the Lost River Range, the Lemhi Range, and the Beaverhead Mountains of the Bitterroot Range as shown in Figure 2-2. A relief of 1,188 to 1,306 m (3,960 to 4,620 ft) exists between the ranges and the relatively flat plain (Hull 1989). Saddle Mountain Peak, near the southern end of the Lemhi Range, reaches an altitude of 3,243 m (10,810 ft) and is the highest point in the immediate INEEL area.

The portion of the SRP occupied by the INEEL may be divided into three minor physical provinces. The first province is a central trough, often referred to as the Pioneer Basin, that extends to the northeast through the INEEL. Two flanking slopes descend to the trough, one from the mountains to the northwest and the other from a broad ridge on the plain to the southeast. The slopes on the northwestern flank of the trough are mainly alluvial fans originating from sediments of Birch Creek and the Little Lost River. Also forming these gentle slopes are basalt flows that have spread onto the plain. The landforms on the southeast flank of the trough are formed by basalt flows, which spread from an eruption zone that extends northeastward from Cedar Butte (Figure 2-1). The lava that erupted along this zone built up a broad topographic swell directing the Snake River to its current course along the southern and southeastern edges of the plain (Figure 2-2). This topographic swell effectively separates the drainage of mountain ranges northwest of the INEEL from the Snake River.

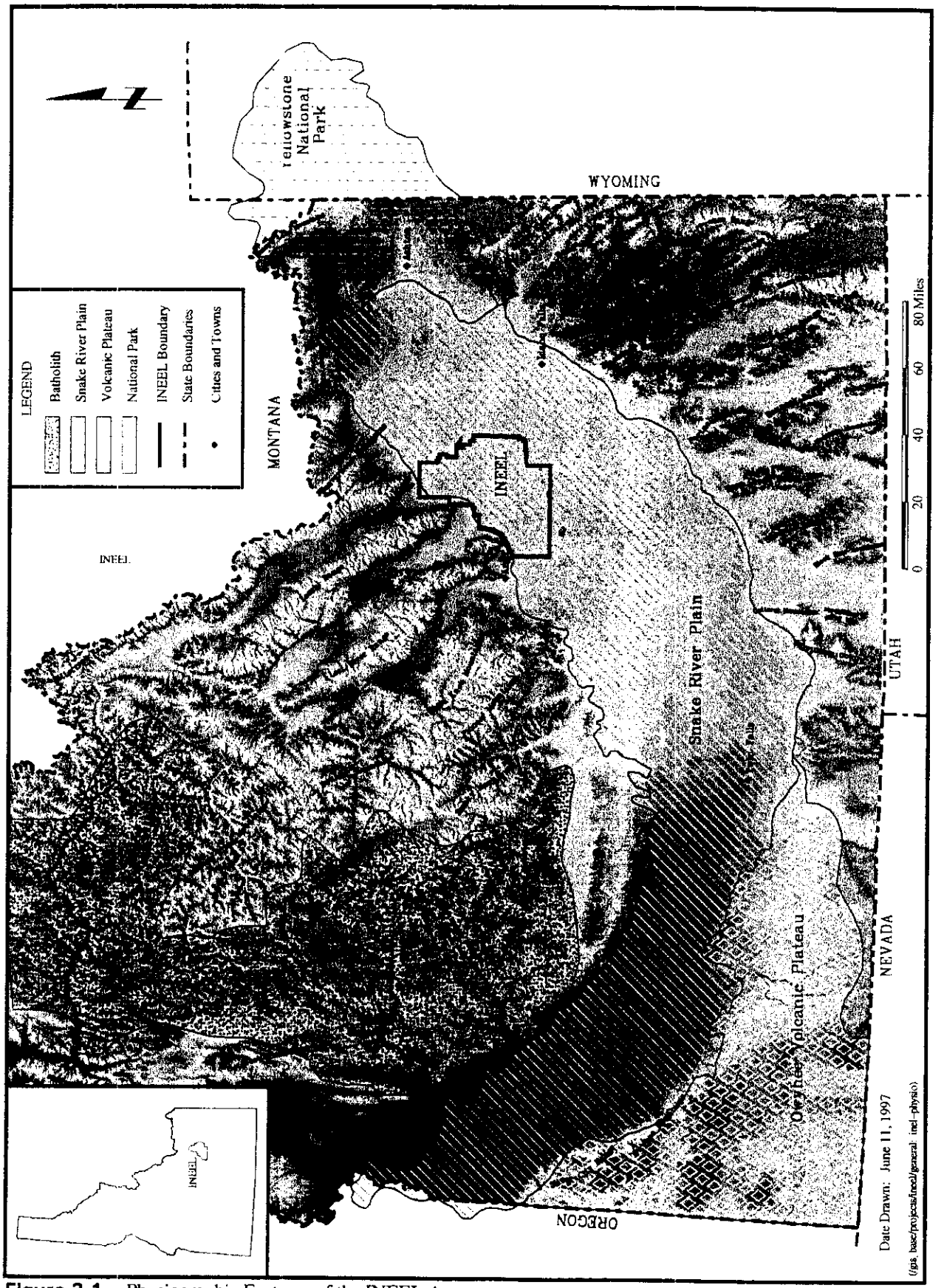

Figure 2-1. Physiographic Features of the INEEL Area.

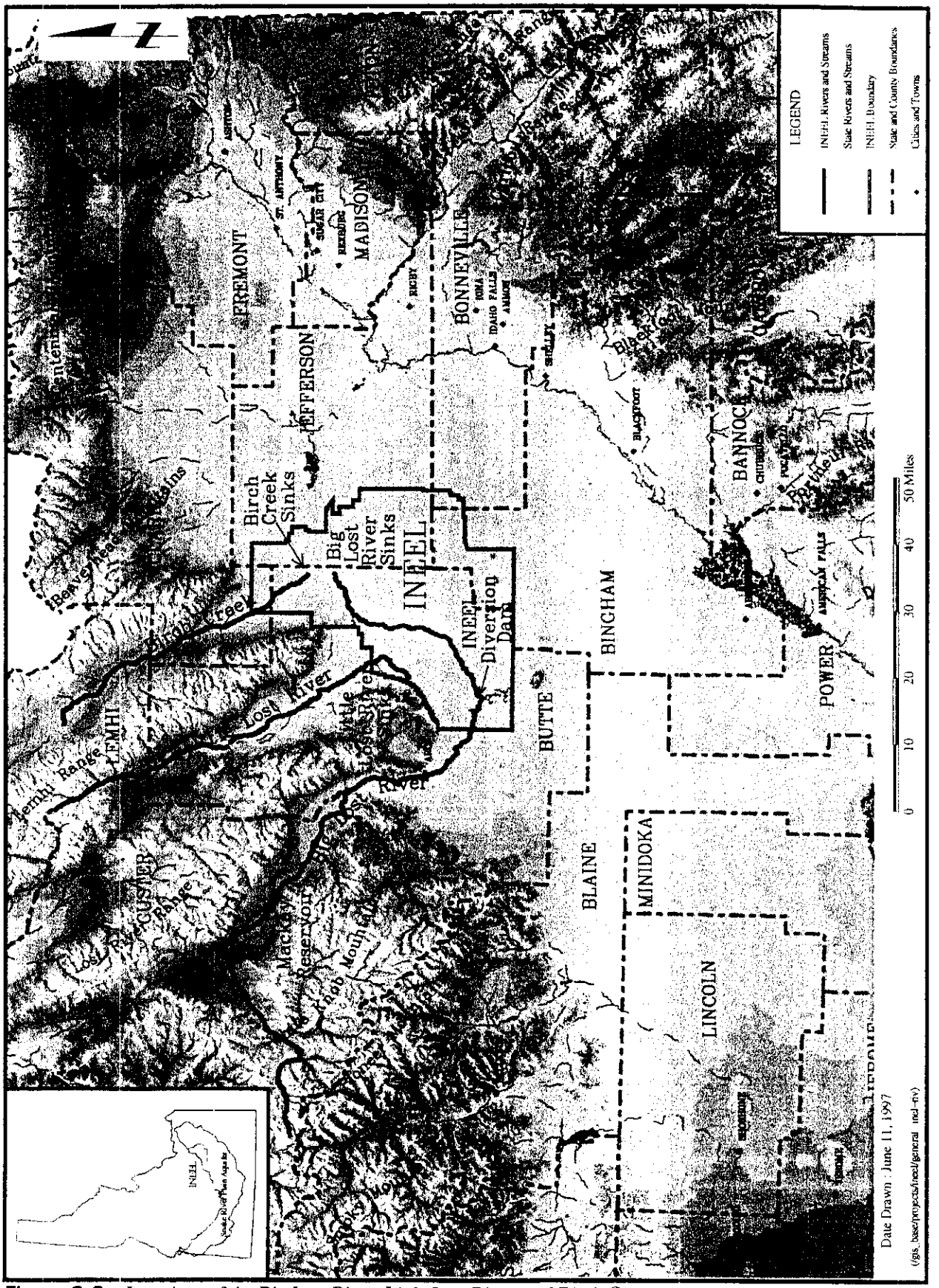

Figure 2-2. Locations of the Big Lost River, Little Lost River, and Birch Creek.

The central lowland of the INEEL broadens to the northeast and joins the extensive Mud Lake Basin. The Big and Little Lost Rivers and Birch Creek drain into this trough from valleys between the mountains to the north and west. The intermittently flowing waters of the Big Lost River have formed a flood plain in this trough, consisting primarily of fine sands, silt, and clay. The streams flow to the Lost River and Birch Creek Sinks, a system of playa depressions in the west-central portion of the INEEL. Test Area North (TAN) is located between the Birch Creek and Lost River Sinks.

2.2 Meteorology

Atmospheric transport of contaminants is controlled by the following physical parameters: particle size, climate, local meteorology, local topography and large structures or buildings on-Site, and contaminant source strength. This section describes the aspects of the physical parameters that are necessary to evaluate environmental and human health impacts from atmospheric transportation of contaminants from TAN.

2.2.1 Climate

In 1949, the U.S. Weather Bureau, by agreement with the U.S. Department of Energy (DOE), established a complete Weather Bureau Station at the INEEL [then the National Reactor Testing Station (NRTS)]. Wind direction and speed, air temperature, and precipitation have been continuously recorded from 1949 or 1950 at the Central Facilities Area (CFA). Recordings of weather conditions on a lesser scale have also occurred at TAN. Most of the information presented in this section is summarized from *Climatology of the INEL* (Clawson et al. 1989) that compiles results of weather recordings for the period 1949 to 1988. Further details of the INEEL and TAN meteorology can be obtained from this reference.

The longest and most complete record of meteorological observations at the INEEL is from the CFA station. Air mass characteristics, proximity to moisture sources, angle of solar incidence, and temperature effects caused by latitude differences would be expected to be alike for all locations at the INEEL, making it possible to extrapolate most meteorological data from CFA to TAN. Additionally, TAN and CFA are at approximately the same terrain elevation and have similar exposure to wind, snow cover, and cloud cover.

The climate at the INEEL is influenced by the regional topography and upper-level wind patterns over North America. The Rocky Mountains and the SRP help to create a semiarid climate with an average summer daytime maximum temperature of 28°C (83°F) and an average winter daytime maximum temperature of -0.5°C (31°F). Infrequent cloud cover over the region allows intense solar heating of the ground surface during the day and the low absolute humidity allows significant radiant cooling at night. These factors create large temperature fluctuations near the ground (Bowman et al. 1984). During a 22-year period of meteorological records (1954 through 1976), temperature extremes at the INEEL have varied from a low of -41°C (-43°F) in January to a high of 39°C (103°F) in July.

2.2.2 Local Meteorology

The average relative humidity at the INEEL ranges from a monthly average minimum of 15% in August to a monthly average maximum of 81% in February and December. The relative humidity is directly related to diurnal temperature fluctuations. Relative humidity reaches a maximum just before sunrise (the time of lowest temperature) and a minimum in the late afternoon (time of maximum daily temperature) (Van Deusen and Trout 1990).

Average annual precipitation at the INEEL is 21.5 cm (8.5 in.). The highest precipitation rates occur during the months of May and June and the lowest rates are in July. Snowfall at the INEEL ranges from a low of about 30.5 cm (12 in.) per year to a high of about 127 cm (40 in.) per year, with an annual average of 66 cm (26 in.). Normal winter snowfall occurs from November through April, though occasional snowstorms occur in May, June, and October (Van Deusen and Trout 1990).

A statistical analysis of precipitation data from CFA for the period 1950 through 1990 was made to determine estimates for the 25- and 100-year maximum 24-hour precipitation amounts and also 25- and 100-year maximum snow depths (Sagendorf 1991). Results from this study indicate 3.43 cm (1.35 in.) of precipitation for a 25-year, 24-hour storm event, and 4.1 cm (1.6 in.) of precipitation for a 100-year, 24-hour storm event. The expected 25-year maximum snow depth is 57.4 cm (22.6 in.) and the 100-year maximum snow depth is 77.8 cm (30.6 in.).

Potential annual evaporation from saturated ground surface at the INEEL is approximately 91 cm (36 in.). Eighty percent of this evaporation occurs between May and October. During the warmest month (July), the potential daily evaporation rate is approximately 0.63 cm/day (0.25 in./day). During the coldest months (December through February), evaporation is low and may be insignificant. Actual evapotranspiration by native vegetation on the INEEL parallels the total annual precipitation input. Potential evapotranspiration is at least three times greater than actual evapotranspiration (Kaminsky et al. 1993).

The local meteorology is influenced by local topography, mountain ranges, and large-scale weather systems. The orientation of the bordering mountain ranges and the general orientation of the ESRP play an important role in determining the wind regime. The INEEL is in the belt of prevailing westerly winds, which are normally channeled across the ESRP. This channeling usually produces a west-southwest or southwest wind. When the prevailing westerlies at the gradient level [approximately 1,500 m (5,000 ft) above land surface] are strong, the winds channeled across the ESRP between the mountains become very strong. Some of the highest wind speeds at the INEEL have been observed under these meteorological conditions. The greatest frequency of high winds occur mainly in the spring.

Local mountain and valley features exhibit a strong influence on the wind flow under other meteorological conditions. The wind directions at TAN are modified somewhat by the proximity of the complex to the broad northwest-trending Birch Creek valley. This causes the normal southwesterly flow to be diverted to a south-southwesterly flow and can sometimes produce a strong component of wind flow from the north-northwest (down the Birch Creek valley). Reverse flows are from a northerly to north-northeasterly direction.

Average monthly wind speeds near-surface [6 m (20 ft)] height are highest in the month of April with speeds of 15.3 km/h (9.3 mph) at CFA and 15.3 km/h (9.5 mph) at TAN. The highest hourly wind speeds recorded at CFA and TAN are 108 km/h (67 mph) and 100 km/h (62 mph), respectively.

The INEEL is subject to severe weather episodes throughout the year. Thunderstorms with highly unlikely tornadoes are observed mostly during the spring and summer. The tornado risk probability at the INEEL is about 7.8×10^{-5} per year (Bowman et al. 1984). An average of two to three thunderstorms occur during each of the months from June through August. Thunderstorms may be accompanied by strong, gusty winds that may produce local dust storms. Occasionally, rain in excess of the long period average monthly total precipitation may be recorded at a monitoring station on the INEEL resulting from a single thunderstorm (Bowman et al. 1984). Precipitation from thunderstorms at the INEEL is generally light.

Dust devils are also common in the region. Dust devils can entrain dust and pebbles and transport them over short distances. They usually occur on warm sunny days with little or no wind. The dust cloud may be several hundred yards in diameter and extend several hundred feet in the air (Bowman et al. 1984).

The vertical temperature and humidity profiles in the atmosphere determine the atmospheric stability. Stable atmospheres are characterized by low levels of turbulence and less vertical mixing. This results in higher ground-level concentrations of emitted contaminants. The stability parameters at the INEEL range from extremely stable to very unstable. The stable conditions occur mostly at night during strong radiant cooling. Unstable conditions can occur during the day when there is strong solar heating of the surface layer or whenever a synoptic scale disturbance passes over the region.

2.3 Geology

The geology of the INEEL is strongly influenced by volcanic and seismic processes that have created the ESRP and the surrounding basin and range structures. The current theory of the evolution of the ESRP volcanic province is that it was formed in response to movement of the North American continent over a deep-seated plume of anomalously hot mantle rocks (hotspot) that now resides beneath Yellowstone National Park (Armstrong, Leeman, and Malde 1975, Pierce and Morgan 1992). Movement of the continent and northeast-directed extension of the crust caused both the ESRP and the northeastern Basin-and-Range province to develop during the past 17 million years. During that time, extension of the crust has produced northwest trending normal faults and mountain ranges, while volcanic activity associated with the Yellowstone Plateau hotspot has produced a belt of calderas along the ESRP. The Yellowstone hotspot was beneath the INEEL area approximately 6.5 to 4.3 million years ago and produced the Tertiary calderas and volcanic fields shown on Figure 2-3. These calderas and their associated explosive rhyolitic volcanism became extinct as the continent moved southwestward over the hotspot. The Pleistocene calderas of the Yellowstone Plateau formed from 2.1 to 0.6 million years ago, and strong geothermal activity continues as the hotspot still resides beneath the Yellowstone Plateau.

2.3.1 Regional Geology

The INEEL is located on the northern edge of the ESRP, a 87-km (54-mi) wide, elongated northeast-trending volcanic province extending from the vicinity of Twin Falls on the southwest to Yellowstone National Park on the northeast. The ESRP lies within the northeastern part of the Basin-and-Range province of southern Idaho, and extends to the basin and range formations on the northwest and southeast. The basin and range formations either terminate at the margin of the plain or extend only a few miles into the plain (Mabey 1982). Compared with the Western SRP, the ESRP has not subsided greatly and is actually rising near its eastern tip (Leeman 1982).

The mountain ranges north of the ESRP are the Lemhi, Beaverhead, and Lost River (Figure 2-2). These ranges are composed of Paleozoic sedimentary rocks that were folded and faulted along the northeastward-trending axis during late Cretaceous or early Tertiary Laramide Orogeny. Many of these Paleozoic rocks dip toward the axis of the ESRP (Nace et al. 1975). Within the margins of the ESRP, Miocene and younger volcanic rocks rest unconformably on the deformed or tilted sedimentary and plutonic rocks ranging in age from Precambrian to Mesozoic and on faulted remnants of middle to late Eocene "calcalkalic" volcanic rocks (Leeman 1982).

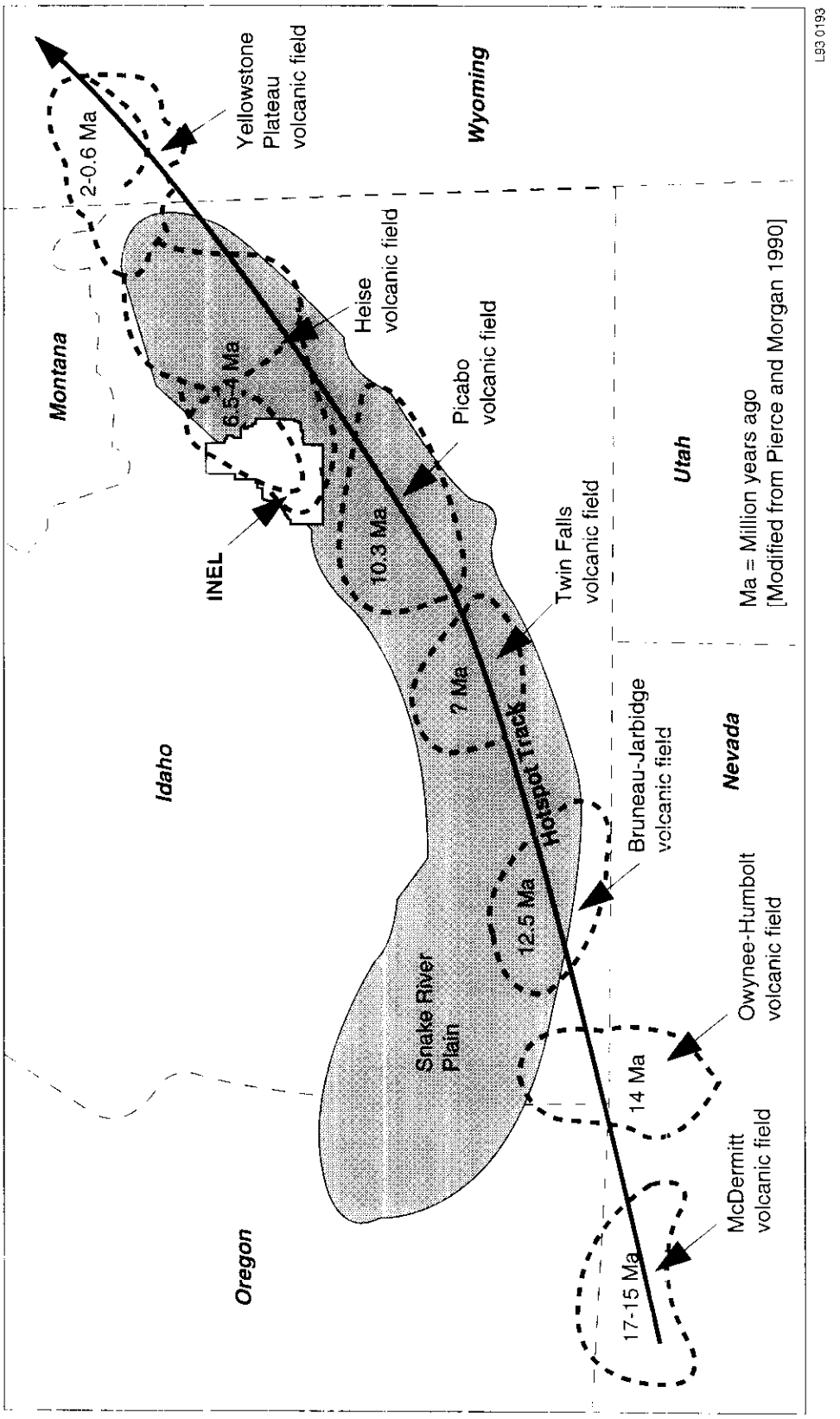

Figure 2-3. Yellowstone plateau hotspot track and resulting volcanic fields.

During the past 4 million years, the ESRP, including the INEEL area, has experienced continued volcanic activity, mostly in the form of small outpourings of basaltic lava flows (Kuntz 1992). Vents for the basaltic volcanism are concentrated in northwest trending volcanic rift zones and along the Axial Volcanic Zone (Figure 2-4). Sediments deposited from wind action, streams and lakes have also accumulated in the ESRP, concurrent with the basaltic lava flows. Lithologic logs of four INEEL deep holes > 610 m (> 2,000 ft) deep including INEL-1 (Figure 2-5), which is a deep geothermal test well, and hundreds of shallower drill holes show that an interlayered sequence of basaltic lava flows and poorly consolidated sedimentary interbeds occur to depths of about 2,500 to 3,700 m (8,200 to 12,100 ft) beneath the INEEL. This sequence is underlain by a large, but unknown thickness of rhyolitic ash flow deposits related to the extinct Tertiary calderas.

Approximately 1.2 million years ago, rhyolite dome building was a minor style of volcanic activity along the Axial Volcanic Zone. Big Southern Butte (0.3 million years ago), East Butte (0.6 million years ago) (Figure 1-1), and an unnamed dome between East Butte and Middle Butte (1.2 million years ago) are all rhyolite domes (Kuntz et al. 1990). In addition, a rhyolite dome occurs in the Cedar Butte volcanic system (0.4 million years ago) and probably beneath Middle Butte (age unknown) (Kuntz et al. 1990).

Much of the INEEL is covered by unconsolidated surficial deposits of various ages and origins. A wide band of Quaternary alluvium extends along the course of the Big Lost River from the southwestern corner of the INEEL to the Lost River sinks area in the north-central portion of the INEEL. Lacustrine (lake) deposits of clays, silts, and sands deposited in Pleistocene Lake Terreton occur in the northern part of INEEL. Loess deposits (wind-deposited silts) cover much of the basalt bedrock of INEEL to thicknesses of up to approximately 6 m (20 ft). Beach sands deposited at the high stand of Lake Terreton were reworked by winds in late Pleistocene and Holocene time and form large dune fields (eolian deposits) in the northeastern part of INEEL (Scott 1982). Large alluvial fans occur in limited areas along the northwest and west boundaries of the INEEL at the base of the Arco Hills and the Lemhi Range.

Bedrock outcrops on and near the INEEL consist mostly of Quaternary basalt lava flows ranging in age from less than 15,000 to greater than 730,000 years (Kuntz et al. 1990). Paleozoic limestones and late-Tertiary rhyolitic volcanic rocks at the south ends of the Lost River Range (Arco Hills) and the Lemhi Range occur in small areas along the northwest margin of the INEEL. Several Quaternary rhyolite domes occur along the Axial Volcanic Zone near the south and southeast borders.

The 1,000-to-2,000-m (3,280-to-6,560-ft) thick sequence of basalt lava flows and sedimentary interbeds that characterize the ESRP (the Snake River Group of Malde 1991) makes up the vadose zone, aquifer, and subaquifer rocks beneath the INEEL. Time stratigraphic rock units in the basalt and sediment sequence range in age from approximately 4 million years at the base to 2,000 years along the Great Rift at the surface (Figure 2-4). The basalt layers between sedimentary interbeds are typically made up of several different lava flows and flow groups that were emplaced over very short periods of geologic time (hundreds to thousands of years). The sedimentary interbeds, although typically thinner than the basalt layers, represent deposition during long periods (10^4 to 10^6 years) of volcanic quiescence (Kuntz 1992).

Because of their mechanism of eruption, flow from the source vents, and cooling after emplacement, the basalt lava flows possess predictable vertical and horizontal facies distributions (Figure 2-6). From bottom to top, basalt lava flows are typically composed of a basal rubble zone, a lower vesicular zone, a massive columnar jointed zone, an upper vesicular and fissured zone, and a cap of platy-jointed crust. From source to distal end, the flows grade from thin, cavernous, platy flows (shelly pahoehoe) with interlayered pyroclastic material to thick units with the vertical zoning described above.

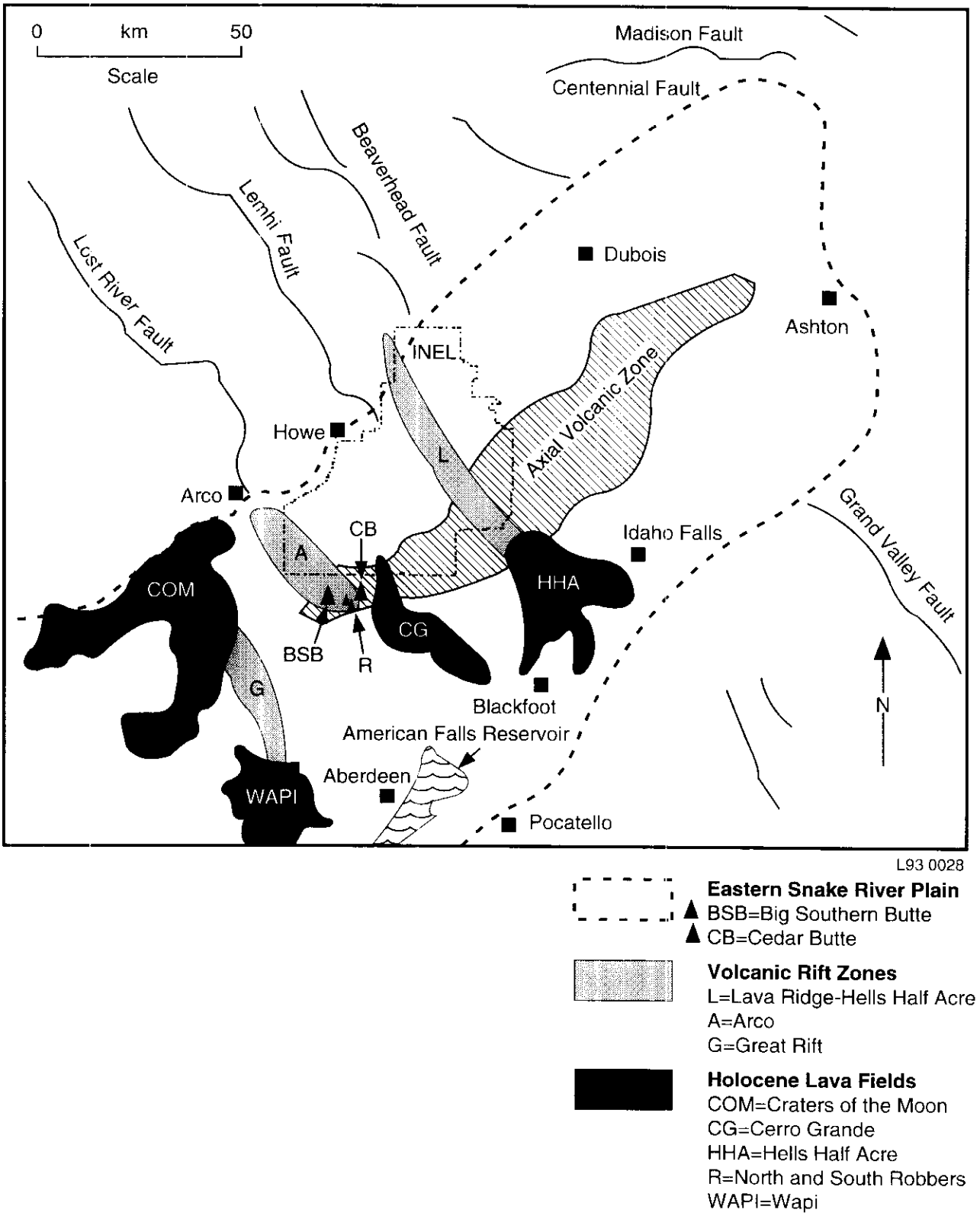

Figure 2-4. Illustration of the axial volcanic flow.

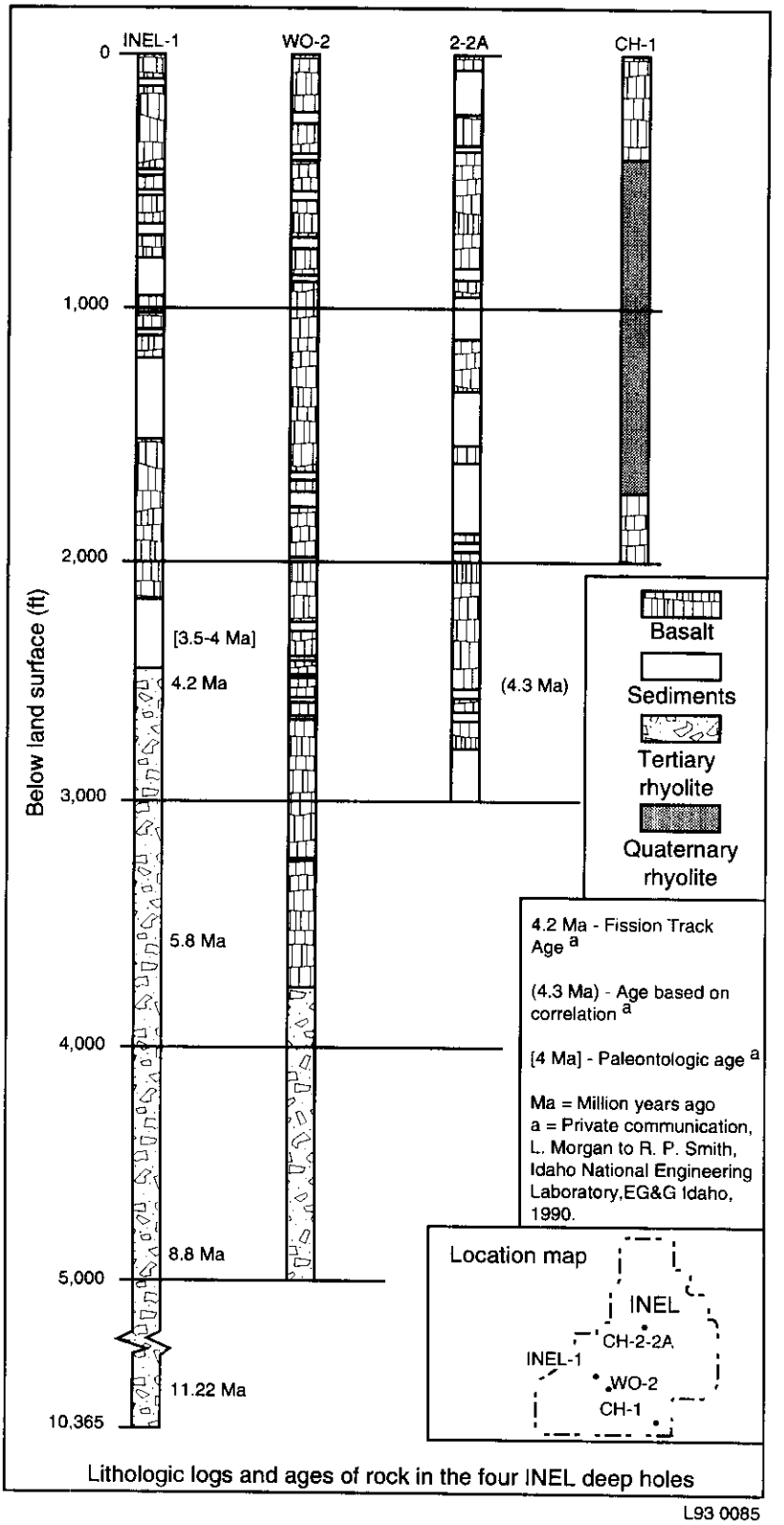

Figure 2-5. Simplified lithologic logs of deep drill-holes on the INEL. (INEL-1 from Doherty et at. 1979; CH-1 from Dohety et al. 1979; CH-1 from Doherty 1979a; 2-2A from Doherty 1979b; and WO-2 from Hackett and Smith 1992).

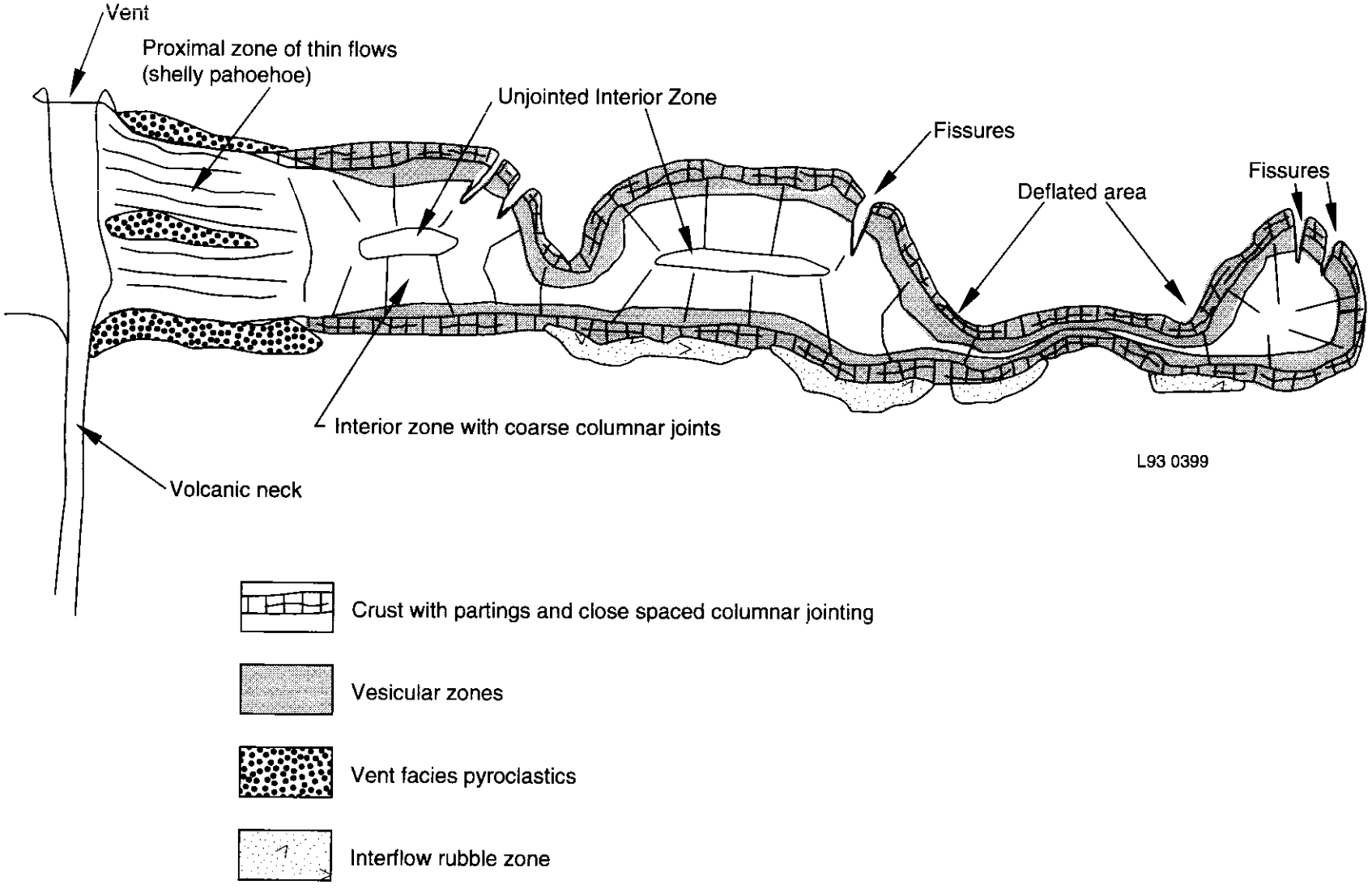

Figure 2-6. Generalized basalt lava flow facies distribution.

In the medial and distal areas, deflation depressions or pits are common and fissures in the broken crust are numerous. Many of the lava flows (especially the larger ones) on the ESRP are fed by lava tubes that commonly drain in the late stages of eruption, leaving long openings in the flows. In the lava flow sequence beneath the ESRP and the INEEL, the basal rubble zones, cooling fractures, fissures, lava tubes, vesicles, cavernous shelly pahoehoe, and pyroclastic zones furnish the porosity and permeability for the storage and transport of water in the aquifer. All of these features are primary (i.e., they were formed during emplacement of the rocks) except the polygonal cooling fractures.

Because of the concentration of volcanic activity along the Axial Volcanic Zone and along volcanic rift zones, these areas tend to be constructional highlands that receive less sediment than other areas. Thus, the total thickness of sediments in the basalt and sediment sequence tends to be greater near the plain margins (Whitehead 1986) and between volcanic rift zones. In fact, many of the drill holes along the Axial Volcanic Zone show that no interbeds occur in that area. The combination of sparse interbeds, and abundance of shelly pahoehoe and pyroclastic material along the Axial Volcanic Zone suggest a thicker and more actively moving aquifer there than elsewhere on the ESRP.

Sediments of diverse origins are interbedded with basalts of the ESRP. The sediments are composed of fine-grained silts that were deposited by wind action; silts, sand, and gravels deposited by streams such as the Big Lost River and in the TAN area, clays, silts, and sands deposited in lakes such as Mud Lake and its much larger Pleistocene predecessor, Lake Terreton. Because the sedimentary depositional processes operating in the geologic past are similar to those operating today, unconsolidated sediments that make up interbeds in the subsurface are similar to those that occur at the surface.

An evaluation was performed of mineralogical similarities in source area rocks and sedimentary deposits at the INEEL (Bartholomay 1990). While large amounts of feldspars and pyroxene in surficial sediment samples from the Big Lost River drainage reflect the large amount of volcanic rocks in the source area, higher amounts of calcite and dolomite in samples from Little Lost River and Birch Creek drainages reflect the abundance of limestone and dolostone in the source areas. A conclusion of the evaluation was that the mineralogy of sedimentary interbeds in the Radioactive Waste Management Complex (RWMC), Test Reactor Area (TRA), and Idaho Chemical Processing Plant (ICPP) areas (Figure 1-2) correlate with sediments of the Big Lost River drainage, and the mineralogy of sedimentary interbeds at TAN correlates with surficial deposits of the Birch Creek drainage. These correlations suggest that the sedimentary interbeds probably were deposited in a depositional environment similar to present-day conditions.

2.3.2 Geology of TAN

The geology of TAN is characterized by basalt flows with sedimentary interbeds overlain by lacustrine sediments from the ancestral Terreton Lake, and playa deposits from both Birch Creek and the Big Lost River (Scott 1982). Figures 2-7 through 2-9 present geologic cross sections through TAN. The locations of the cross sections are shown on Figure 2-10. These cross sections were constructed from lithological and geophysical logging of the various boreholes, coreholes, and wells drilled in the TAN area. Lake floor and playa deposits consist of silty sand to silty clay with poor to moderate sorting, and commonly exhibit both parallel layering and cross bedding. The lacustrine deposits are exposed at the surface in the southeastern portion of TAN. TAN soils were formed as a result of alluvial, eolian, and lacustrine deposition and are derived from silicic volcanic and paleozoic rocks from the nearby mountains and buttes (Nace et al. 1959). U.S. Geological Survey (USGS) cross sections and fence diagrams of (Deutsch, Nace, and Voegeli 1952) show that coarser-grained deposits underlie the silts and silty clays at the surface over much of the area. These deposits are typically clayey silt, with lesser amounts of sand,

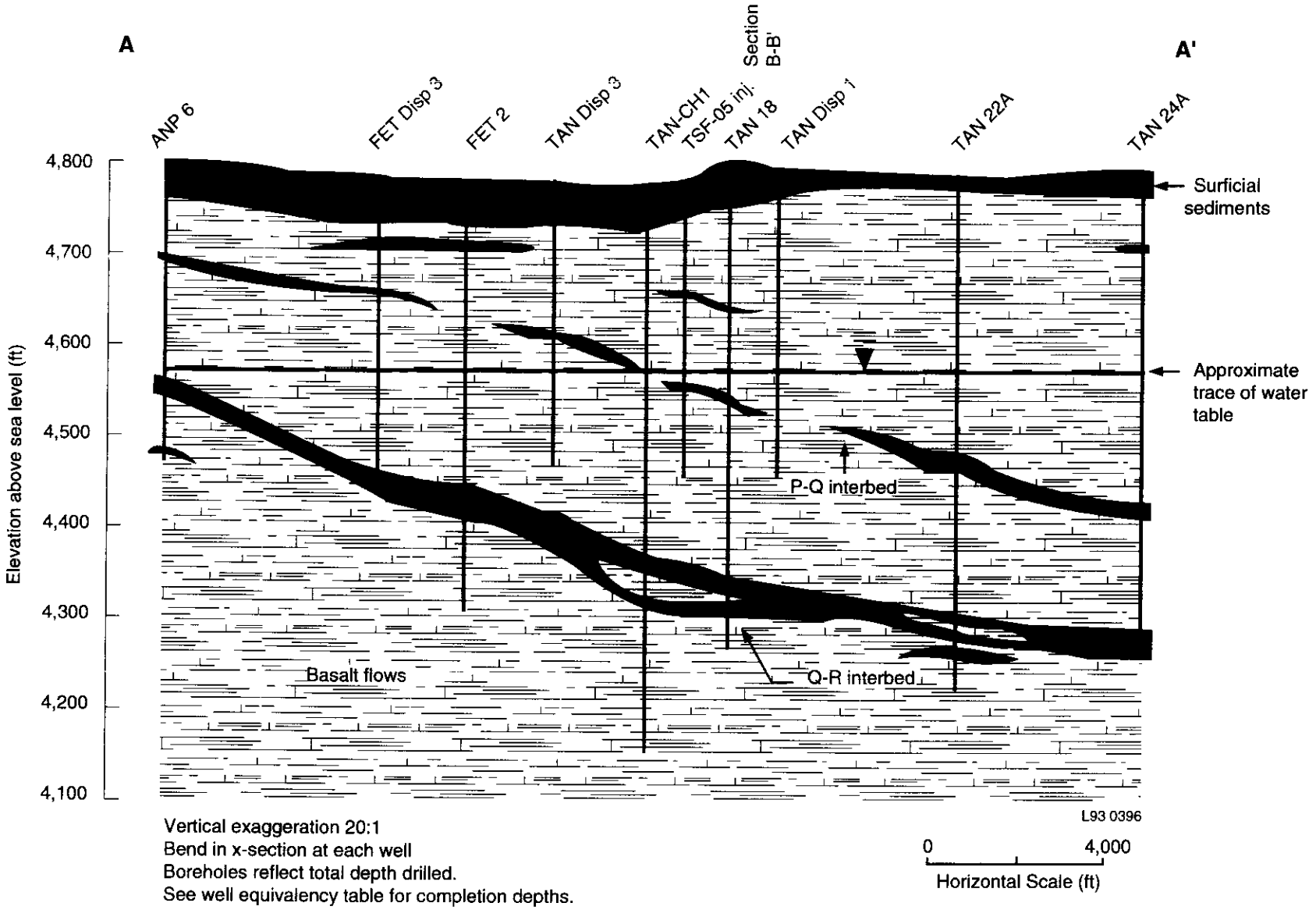

Figure 2-7. Northwest-southeast cross section through TAN (see Figure 2-10 for location).

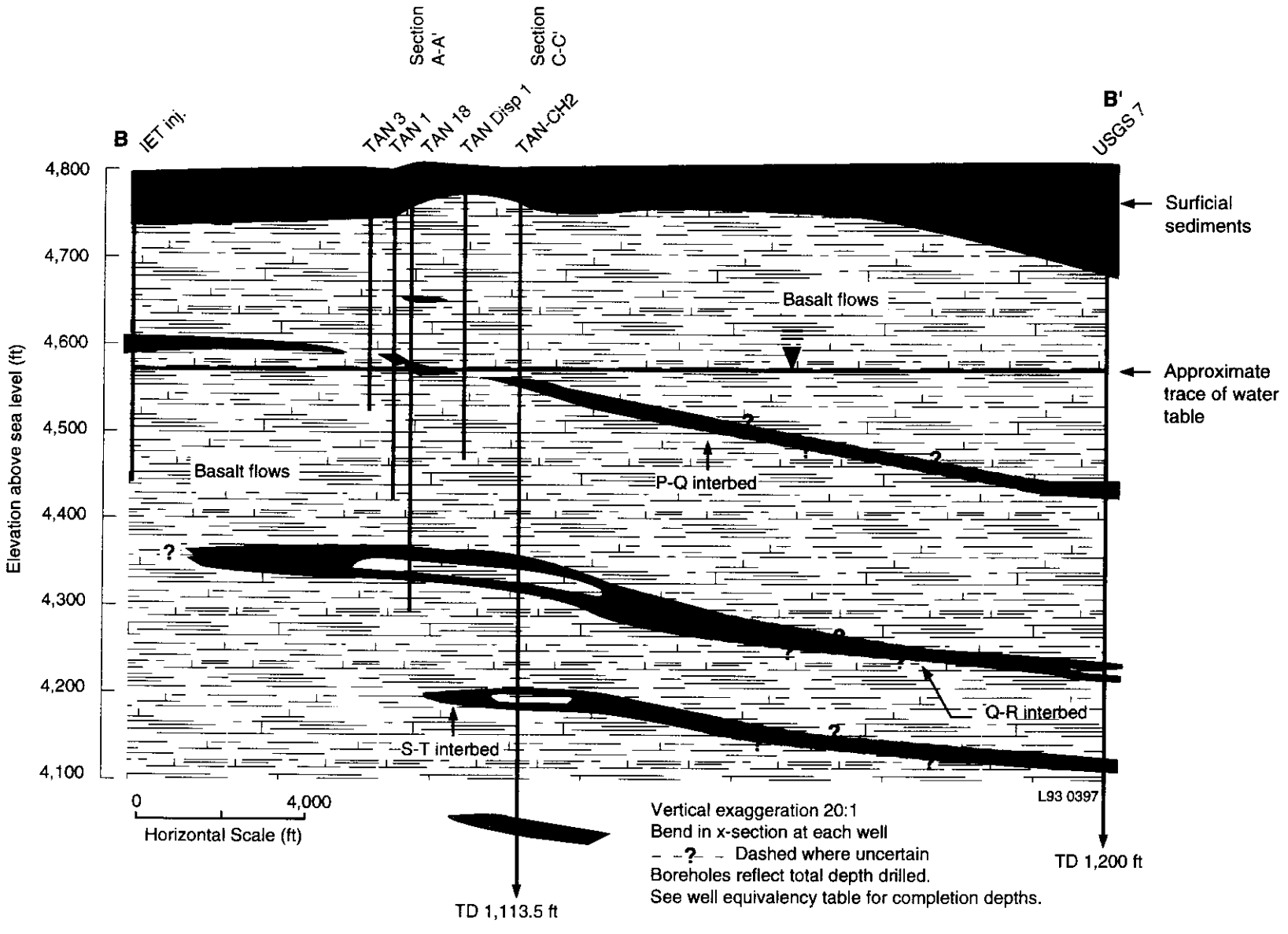

Figure 2-8. Northeast-southwest cross section through TAN (see Figure 2-10 for location).

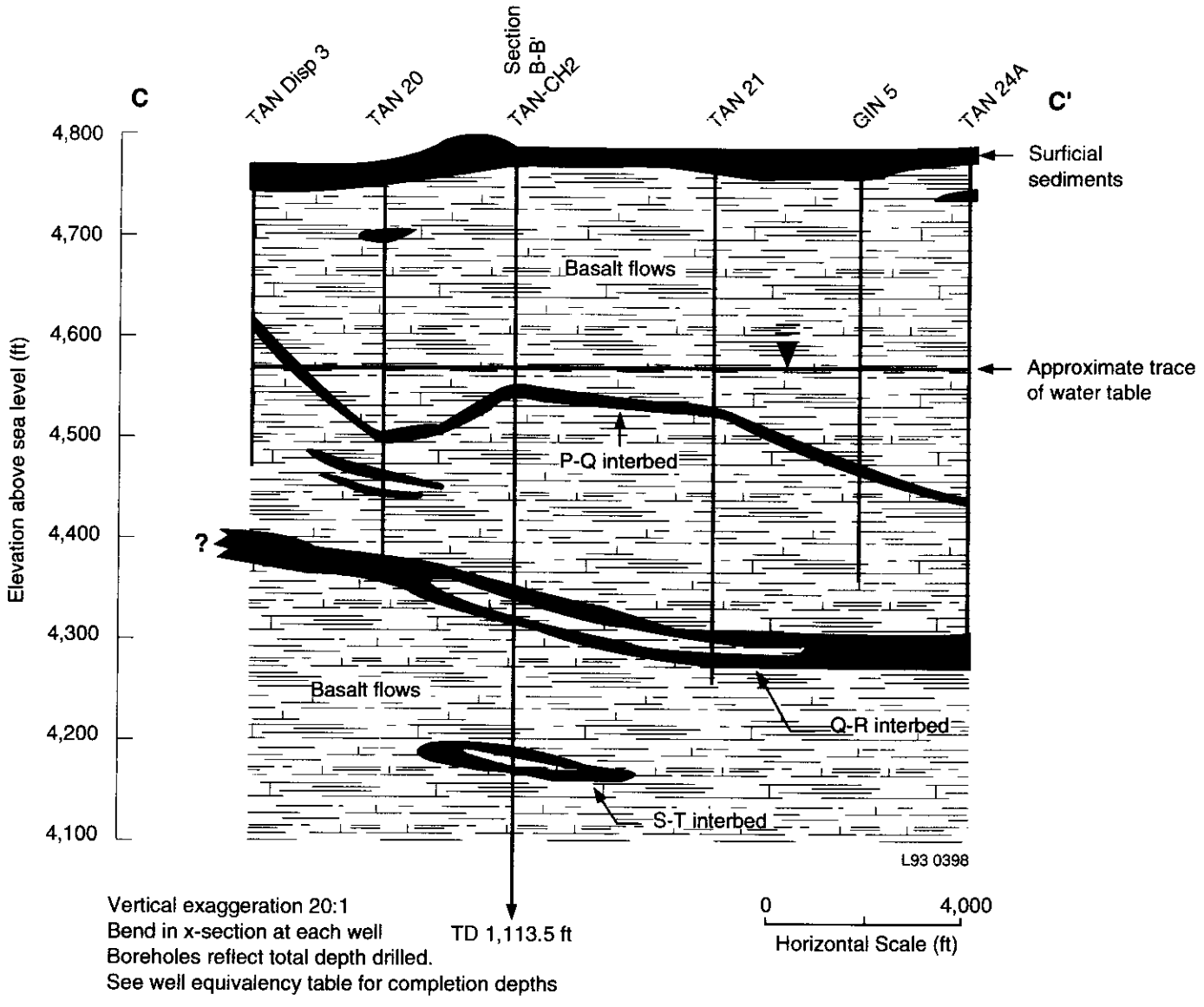

Figure 2-9. South-central northwest-southeast cross section through TAN (see Figure 2-10 for location).

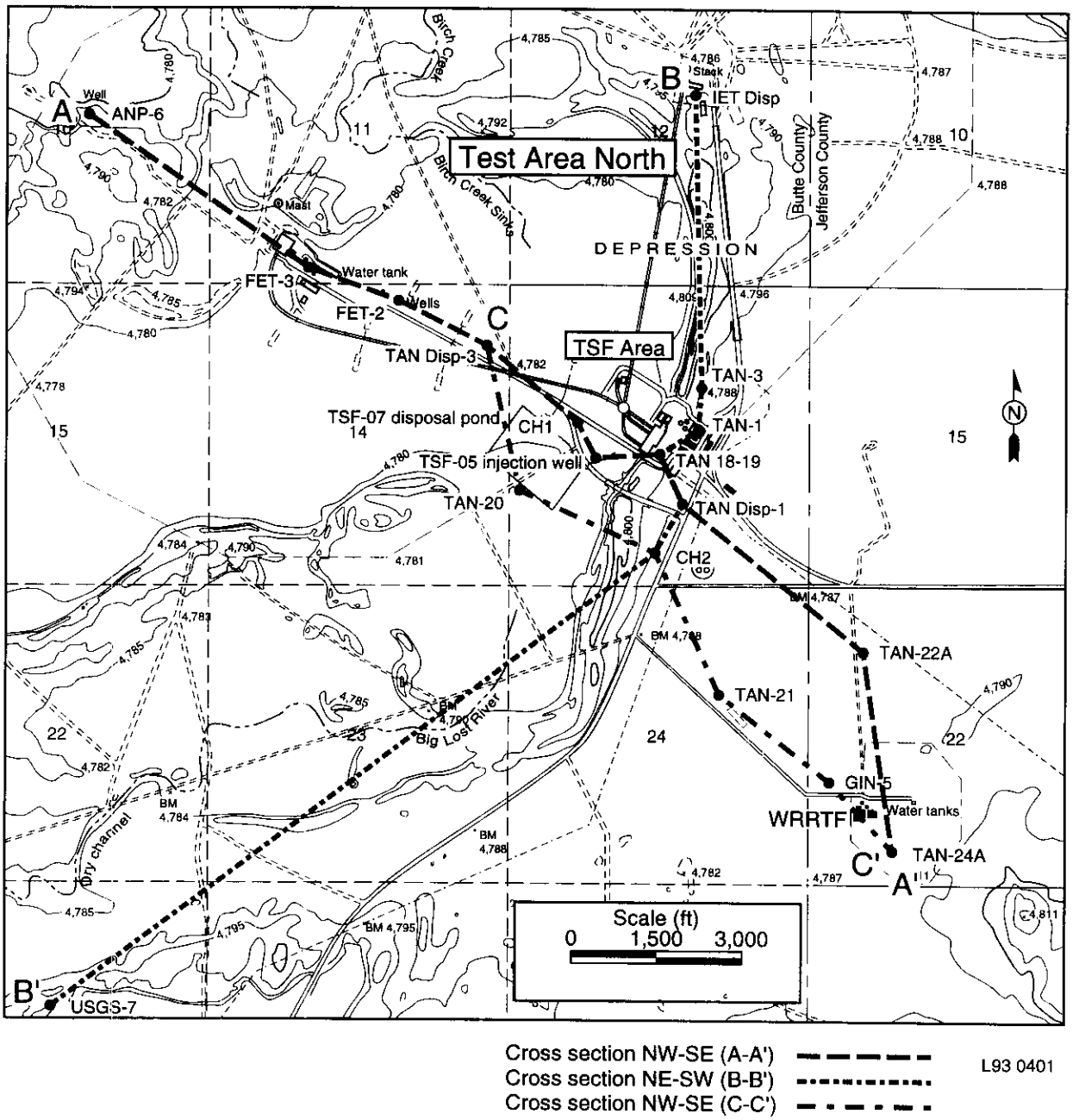

Figure 2-10. Index map showing the locations of cross sections A-A' (Figure 2-7), B-B' (Figure 2-8) and C-C' (Figure 2-9).

fine gravel, clay, and silt (Nace et al. 1959). The sands and gravels could be lake margin deposits that were buried by lake floor deposits in a transgressive sequence as Lake Terreton grew, or they could be Birch Creek alluvial deposits that were buried as the lake grew. Beach and bar deposits are also associated with the Lake Terreton deposits.

Wells drilled at TAN indicate that the thickness of the alluvium generally varies from 1.5 to 23 m (5 to 75 ft) thick, with a decreasing thickness in alluvium to the east. Maximum thicknesses appear to occur southwest of the TAN facility. Surficial sediments also thicken to the north and northwest near the Water Reactor Research Test Facility (WRRTF), and show variable depths within a several thousand foot radius of TAN. The wide variation in the alluvial thickness is caused by the irregular nature of the underlying basalt flows, and measurement of alluvial thickness is somewhat biased by the number and spacing of boreholes. Rock outcrops are common and some soils are relatively shallow.

The basalt underlying the surficial sediments is a very dark, hard, tholeitic basalt that shows distinct hexagonal jointing, as observed in excavations (Nace et al. 1959). Geologic descriptions from wells drilled in the TAN area indicate that the basalt exhibits a wide range of lithologic textures and structures, from dense to highly vesicular basalt to massive to highly fractured basalt. Individual flow units have a median thickness of approximately 4.5 m (15 ft). The underlying interbeds at TAN, with a median thickness of approximately 1.2 m (4 ft), are much thinner than interbeds found elsewhere on the INEEL, with a median thickness of approximately 3 m (10 ft).

Borehole televiewer logging of wells in the vicinity of TAN provides a detailed look at the lithostratigraphy and fracturing within the basalts beneath the ESRP. At the base of each flow is generally a narrow zone of rubbly material, which grades into a massive interior cut by near-vertical fractures or possibly columnar joints. Near the top is a narrow zone a few feet thick of shallow dipping fractures. This pattern of fractures in the basalts is most likely caused by thermal stresses generated during cooling. Flows identified on the basis of this characteristic pattern have a thickness of up to 26 m (85 ft) (Moos and Barton 1990). Specific flow units were not positively correlated between wells.

Several lithologic types were encountered in interbeds within the basalt. Sedimentary interbeds of clay and silt material that often contain cluster basalt, and interbeds consisting of basaltic breccia supported by a matrix of scoriaceous rubble are most common. The least common interbed is composed of sandy material.

Using available geologic and geophysical data from wells drilled at TAN, numerous interbeds have been identified. Two of these interbeds, referred to as the P-Q and Q-R interbeds, can be consistently correlated throughout the area at this time. The P-Q and Q-R interbeds both consist of clay or silt. The P-Q interbed has been encountered in approximately 50% of the wells drilled deeply enough to intersect the interbed and, therefore, it appears to be laterally discontinuous. Based on the results of deeper boring, the Q-R interbed appears to be more laterally continuous in the TAN area. The depth to the top of the Q-R interbed increases from northwest to southeast. The thickness of the Q-R interbed is approximately 12 m (40 ft). The interbed is split in some wells by a basalt unit ranging from 0.9 to 9 m (3 to 30 ft) thick (Kaminsky et al. 1993).

2.4 Hydrology

This section provides (1) an overview of the hydrology at the INEEL and a discussion of the hydrology in the vicinity of TAN, (2) a summary of previous work performed by both the USGS and site

contractors, and significant data obtained during investigations of TAN groundwater for Operable Unit (OU) 1-07B.

2.4.1 Surface Water Hydrology

Most of the INEEL is located in a topographically closed drainage basin into which the Big Lost River, Little Lost River, and Birch Creek drain during significant runoff (Figure 2-2). These streams drain mountain watersheds to the north and west of the INEEL, including the Pioneer, Lost River, Lemhi, and Bitterroot mountain ranges. Rainfall and snowmelt within the upper watershed contribute to surface water, mainly during springtime. Average annual discharge, upstream of the INEEL, for the Big Lost River (below the Mackay Dam), Little Lost River, and Birch Creek are 314 cubic feet per second (ft^3/s), 70 ft^3/s, and 78 ft^3/s, respectively (DOE 1991).

The Big Lost River and Birch Creek are the only natural surface water features of concern near TAN. TAN is located between the terminus of the Big Lost River and the terminus of Birch Creek. Local surface runoff from surrounding slopes during the snowmelt season or during a heavy thunderstorm may also contribute to the surface water at TAN.

Most of the water in these streams is diverted upstream of the INEEL for irrigation purposes (Bowman et al. 1984) or is lost to the subsurface because of high infiltration rates in the channel bed (Nace et al. 1959). Birch Creek originates from springs below Gilmore Summit in the Beaverhead Mountains and flows in a southeasterly direction onto the SRP. The water in the creek is diverted from the channel 6.4 km (4 mi) upstream of the INEEL northern boundary by a canal for irrigation and hydropower uses. Flows not used for irrigation during the off-season, usually early November through mid-April, are returned to the main Birch Creek channel within the INEEL boundary. The channel leads to a gravel pit near Playa 4, located 6.4 km (4 mi) north of the main facilities at TAN, where it infiltrates the gravel pit bottom. Water was observed flowing in this area of the Birch Creek channel during early April 1992. If the flow is continuous throughout the winter season, the water readily infiltrates the channel and gravel pit bottom. However, if the flow is interrupted, the channel and pit bottom may freeze, reducing infiltration rates. In this event, a second channel is used to divert the flows to a second gravel pit, located to the east away from the TAN facilities.

The Big Lost River is the principal surface-water feature of the INEEL. Several storage and diversion systems exist on the Big Lost River. The Mackay Dam, which was completed in 1917, is located 30 mi upstream of Arco, Idaho, and has a storage capacity of 44,500 acre-ft (Van Haaften, Koslow, and Naretto 1984). Between the dam and the SRP, a number of irrigation diversions exist. No surface outflow leaves the INEEL, except for minor local slope runoff (Nace et al. 1959).

2.4.2 Regional Groundwater Hydrology

The Snake River Plain Aquifer (SRPA) consists of a series of saturated basalt flows and interlayered pyroclastic and sedimentary materials that underlie the ESRP. The SRPA is approximately 325 km (200 mi) long, 65 to 95 km (40 to 60 mi) wide, and covers an area of approximately 25,000 km^2 (9,600 mi^2). It extends from Hagerman, Idaho, on the west to near Ashton, Idaho, northeast of the INEEL. The Environmental Protection Agency (EPA) designated the SRPA as a sole source aquifer under the Safe Drinking Water Act on October 7, 1991 (194 FR 50634).

Flow within the aquifer lies within macroporous media. Permeability of the aquifer is controlled by the distribution of highly fractured basalt flow tops and interflow zones with some additional permeability

contributed by vesicles and intergranular pore spaces. The variety and degree of interconnected water-bearing zones complicates the direction of groundwater movement locally throughout the aquifer (Barraclough, Lewis, and Jensen, 1981). Although a single lava flow may not be a good aquifer, a series of flows may include several excellent water-bearing zones. If the sequence of lava that flows beneath the SRP is considered to constitute a single aquifer, it is one of the world's most productive (Mundorff, Crosthwaite, and Kilburn 1964).

A USGS report estimated that as much as 2.5×10^{12} m^3 (2 billion acre-ft) of water may be stored in the aquifer, of which approximately 6.2×10^{11} m^3 (500 million acre-ft) are recoverable (Robertson, Schoen, and Barraclough 1974). Later estimates suggest that the aquifer contains approximately 4.9×10^{11} m^3 (400 million acre-ft) of water in storage. The aquifer discharges approximately 8.8×10^9 m^3 (7.1 million acre-ft) of water annually to springs and rivers. Pumpage from the aquifer for irrigation totals approximately 2.0×10^9 m^3 (1.6 million acre-ft) annually (Hackett, Pelton, and Brockway 1986).

Recharge to the SRPA from within INEEL boundaries is primarily in the form of infiltration from the rivers and streams draining the areas to the north, northwest, and northeast of the SRP. In most years, spring snowmelt produces surface runoff that accumulates in depressions in the basalt or in playa lakes. On the INEEL, water not lost to evapotranspiration recharges the aquifer because the INEEL is in a closed topographic depression. Significant recharge from high runoff in the Big Lost River causes a regional rise in the water table over much of the INEEL. Water levels in some wells have been documented to rise as much as 1.8 m (6 ft) following very high flows in the Big Lost River (Pittman, Jensen, and Fischer 1988).

Water table contours for the SRPA below the INEEL are depicted in Figure 2-11. The regional flow is to the south-southwest; though, locally, the direction of groundwater flow is affected by recharge from rivers, surface water spreading areas, pumpage, and inhomogeneities in the aquifer. Across the southern quadrant of the INEEL, the average gradient of the water table is approximately 0.38 m/km (2 ft/mi) (Lewis and Goldstein 1982). The hydraulic gradient for the regional aquifer in the vicinity of TAN is about 0.2 m/km (1 ft/mi) (Lewis and Jensen 1984). Depth to water varies from approximately 60 m (200 ft) in the northeast corner of the INEEL to 305 m (1,000 ft) in the southeast corner. The depth to water at TAN varies from slightly less than 61 m (200 ft) at the TSF-05 injection well to more than 107 m (350 ft) at the Aircraft Nuclear Propulsion (ANP)-7 well, located in the northern portion of TAN.

The thickness of the active portion of the SRPA at the INEEL has been estimated by the USGS to be between 75 and 250 m (250 and 820 ft). Drilling information from INEL-1, a deep geothermal test well located 4 km (2.5 mi) north of TRA, suggests an active flow system thickness of between 134 and 250 m (440 and 820 ft) (Mann 1986). Drilling of TAN-CH2 just south of Technical Support Facility (TSF) suggests that the aquifer thickness in the vicinity of TAN may be greater than 274 m (900 ft).

Studies of drill core from several of the deep exploration drill holes on the INEEL (most notably CH2-2A and WO-2) show that secondary mineralization and alteration significantly reduce the porosity and permeability of basalts at depths of 350 to 550 m (1,200 to 1,800 ft). Geophysical logs also show that water movement and water content drops off rapidly at this depth interval. Together, logs and cores suggest that the bottom of the active portion of the aquifer lies in the depth range of 350 to 550 m (1,200 to 1,800 ft).

Aquifer tests have been conducted on wells in the SRPA to determine whether the wells were suitable for water supply, and in support of regional studies conducted by the USGS (Mundorff, Crosthwaite, and

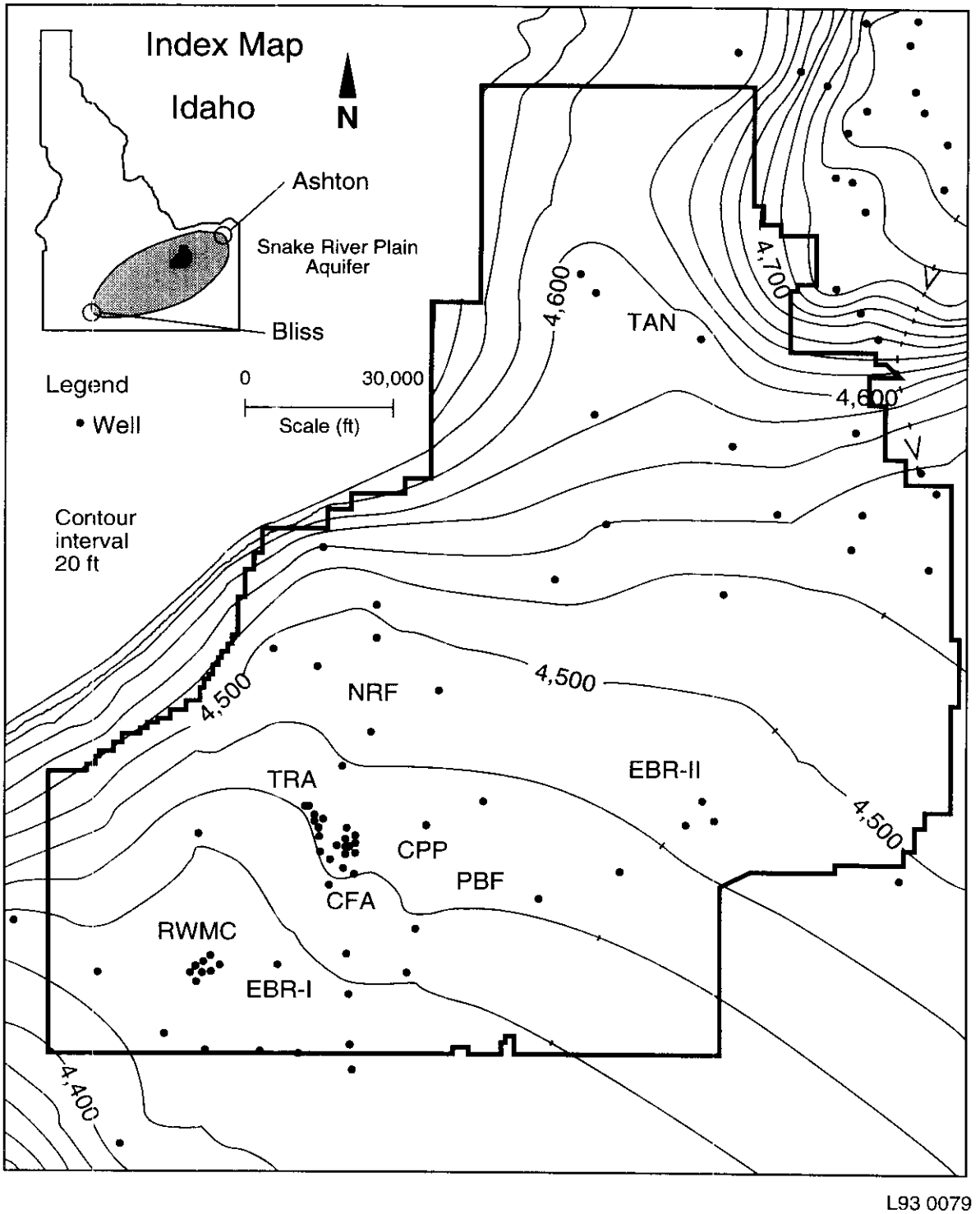

Figure 2-11. Water table contours of Snake River Plain Aquifer.

Kilburn 1964 and Wood 1989). Many tests were conducted by the USGS during the 1950s. Data from those tests, which used high pumping rates, have been compiled and were used to estimate the transmissivity and storage coefficients of the aquifer at TAN. The best transmissivity estimates range from a low of 43 m^2/d (400 ft^2/d) in the TSF-05 injection well to a high of 74,000 m^2/d (800,000 ft^2/d) in the ANP-6 well, with a median value of 3,600 m^2/d (38,500 ft^2/d). These data suggest that wells near TAN have a relatively low transmissivity compared to the regional aquifer transmissivity, which is estimated to be 25,000 to 37,000 m^2/d (270,000 to 400,000 ft^2/d) (Robertson, Schoen, and Barraclough 1974). This is probably because of the short open interval in the wells rather than a local decrease in transmissivity. None of the nine wells tested fully penetrated the aquifer; therefore, the transmissivity of the local aquifer in the vicinity of TAN may be somewhat higher. However, the anomalously low transmissivity of TSF-05 in relation to other TAN wells is likely the result of wastes injected into the aquifer during its operation as a waste injection well. This low transmissivity, if related to the wastes that were injected into the aquifer, will therefore bias the median transmissivity value for TAN to the low side.

2.4.3 TAN Hydrology

Figure 2-12 is a regional water table map of the TAN area showing the inferred direction of groundwater flow for December 1990. A major feature that should be noted in Figure 2-12 is that the regional water-table gradient is very flat in the area of TAN. Under the conditions of a flat water-table gradient, the influence of the production wells on the reported contaminant source (TSF-05 injection well) is strong, and may cause major flow disruptions or reversals in the vicinity of TAN. Pumping of the production wells at TAN causes perturbation to the regional groundwater gradient, which results in localized differences in the water table in the vicinity of TAN. This situation allows the production wells to capture contaminated water originating from the TSF-05 injection well, although inspection of the regional water table map (Figure 2-12) would indicate that the plume would probably not have naturally reached the production wells (Kaminsky et al. 1993). TAN area monitoring wells are identified in Figure 2-13.

The calculated hydraulic conductivity at TAN, based on pumping tests, ranges from a low of 1.5 m/d (5 ft/d) at the TSF-05 injection well to 820 m/d (2,700 ft/d) at well USGS-24 (Wood, Hull, and Doornbos 1989). Slug tests performed on wells at TAN in 1989 and 1990 were analyzed using various techniques to determine the horizontal hydraulic conductivity (Hvorslev 1951; Bouwer and Rice 1976; and van der Kamp 1976). The horizontal hydraulic conductivity values from slug tests range from 0.06 to 150 m/d (0.20 to 500 ft/d). In addition, borehole packer tests using the Neuman and Theis analytical methods were carried out in boreholes drilled in 1992. The results of the slug tests and the aquifer test performed on the TAN wells demonstrate that the aquifer is not homogeneous and isotropic, and that there is considerable variation in the horizontal hydraulic conductivity at TAN (Kaminsky et al. 1993). While data from slug tests conducted at TAN indicate a wide range of hydraulic conductivities in the aquifer, it should be noted that the anomalously low value obtained in TSF-05 is likely the result of past waste injection into the well.

The groundwater flow velocity in the vicinity of TAN is estimated to range from a low of 0.0006 m/d (0.002 ft/d) to a high of 1.3 m/d (4.3 ft/d), with a median value of 0.06 m/d (0.2 ft/d) (Kaminsky et al. 1993). This assumes a low, high, and median transmissivity value of 37, 74,300, and 3,575 m^2/d (400, 800,000, and 38,500 ft^2/d), respectively, and a hydraulic gradient of 0.2 m/km (1 ft/mi), an aquifer thickness of 76 m (250 ft), and a porosity of 0.15. It should be noted that median groundwater flow velocities at TAN are likely impacted by anomalously low values calculated for TSF-05. The low value at TSF-05 is likely the result of past waste injection into the well.

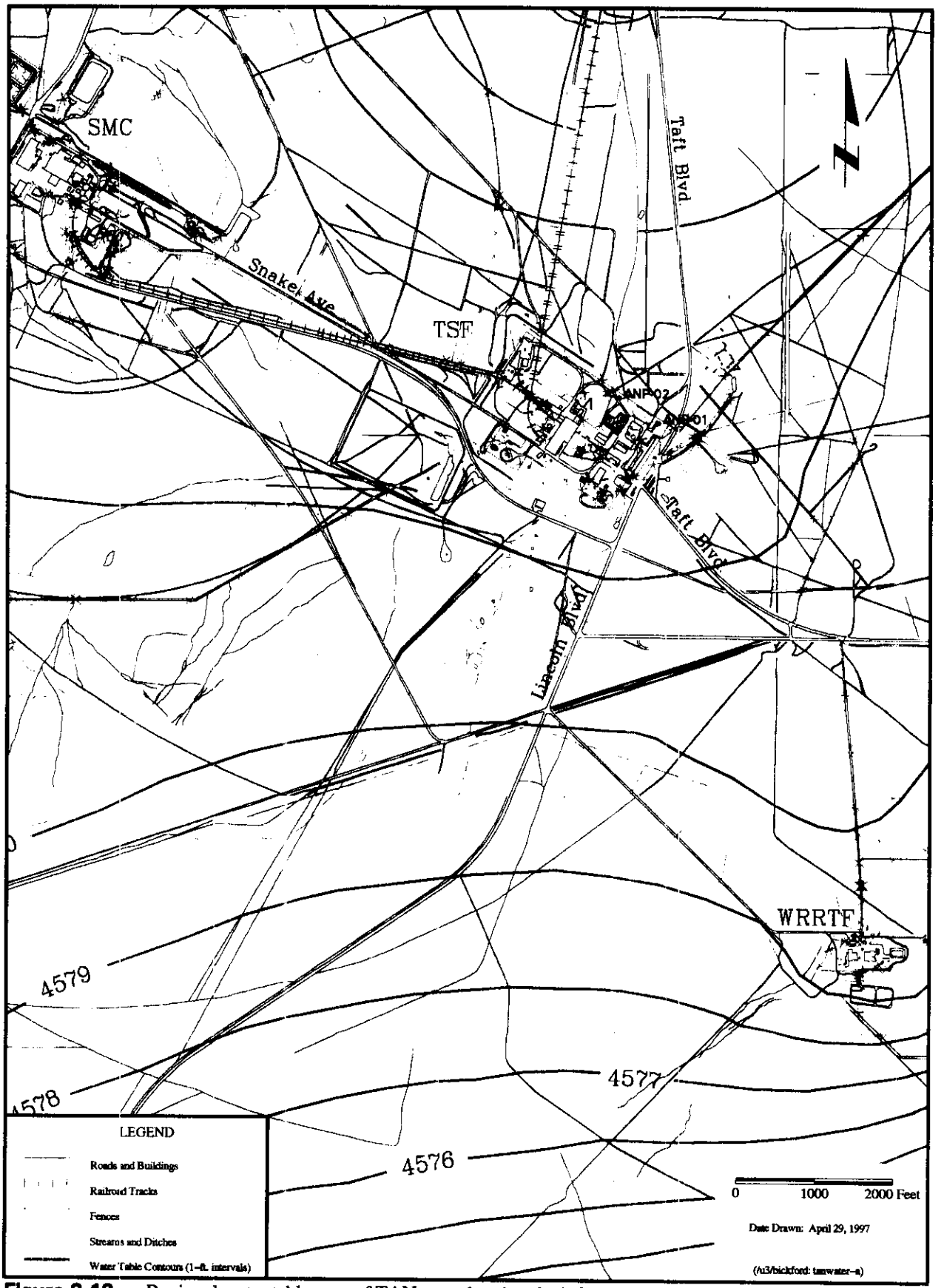

Figure 2-12. Regional water table map of TAN area showing the inferred direction of groundwater flow.

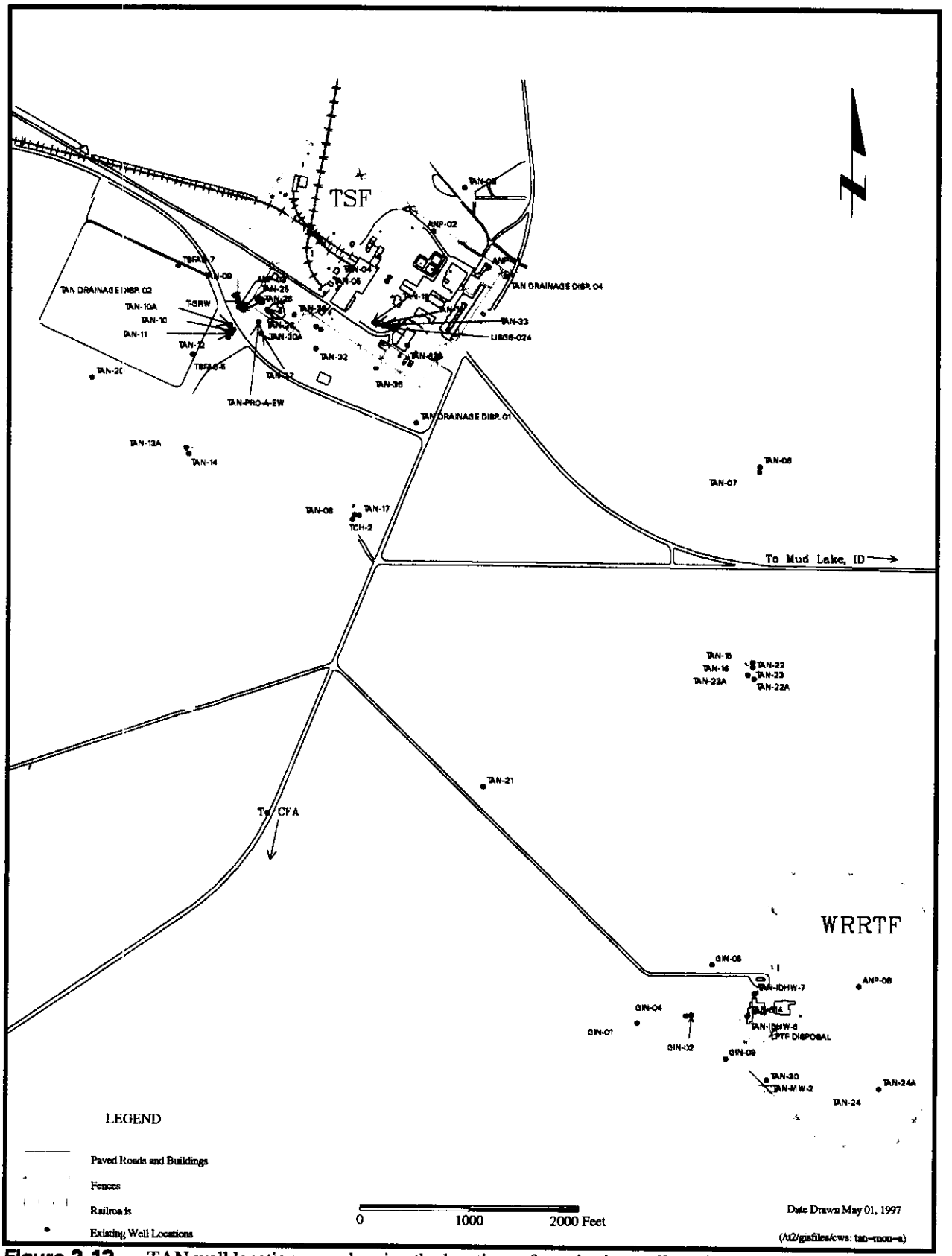

Figure 2-13. TAN well location map showing the locations of monitoring wells and production wells (ANP–02, ANP–01).

Water in the SRPA shows a chemical composition reflecting the source area of the recharge (Robertson, Schoen, and Barraclough 1974). Recharge from the north and northwest is derived from clastic and carbonate sedimentary rocks and is, therefore, a calcium bicarbonate-type water. Recharge from the east is derived from silicious volcanic rocks, and the water is somewhat higher in sodium, fluoride, and silica. The groundwater at TAN is of the calcium bicarbonate-type indicative of recharge from the north and northwest.

2.5 References

Armstrong, R. L., W. P. Leeman, and H. E. Malde, 1975, "K-Ar Dating, Quaternary and Neogene Rocks of the Snake River Plain, Idaho," *American Journal of Science*, pp. 225–251.

Barraclough, J. T., B. D. Lewis, and R. G. Jensen, 1981, *Hydrologic Conditions at the Idaho National Engineering Laboratory, Idaho - Emphasis: 1974-1978*, U.S. Geological Survey Water-Supply Paper 2191.

Bartholomay, R. C., 1990, *Mineralogical Correlation of Surficial Sediment from Area Drainages, with Selected Sedimentary Interbeds at the Idaho National Engineering Laboratory, Idaho*, U.S. Geological Survey Water Resources Investigations Report 90-4147, August 1990.

Bouwer, H., and R. C. Rice, 1976, "A Slug Test for Determining Hydraulic Conductivity of Unconfined Aquifers with Completely or Partially Penetrating Wells," *Water Resources Research*, Vol. 12, pp. 423–428.

Bowman, A. L., W. F. Downs, K. S. Moor, and B. F. Russell, 1984, *INEL Environmental Characterization Report*, Vol. 2, EGG-NPR-6688, September 1984.

Clawson, K. L., G. E. Start, and N. R. Ricks, 1989, *Climatography of the Idaho National Engineering Laboratory*, 2nd ed., DOE/ID-12118, December 1989.

Deutsch, M., R. L. Nace, and P. T. Voegeli, 1952, *Geology, Ground Water, and Waste-Disposal at the Aircraft Nuclear Propulsion Project Site, Idaho*, IDO-220230USGS, U.S. Geological Survey.

DOE, 1991, *Draft Environmental Impact Statement for the Siting, Construction, and Operation of New Production Reactor Capacity*, Vol. 2: Sections 1–6, DOE/EIS-0144D, U.S. Department of Energy, Office of New Production Reactors, April 1991.

Hackett, B., J. Pelton, and C. Brockway, 1986, *Geohydrologic Story of the Eastern Snake River Plain and the Idaho National Engineering Laboratory*, U.S. Department of Energy Idaho Operations, Novernber 1986.

Hull, L. C., 1989, *Conceptual Model and Description of the Affected Environment for the TRA Warm Waste Pond (Waste Management Unit TRA-03)*, EGG-ER-8644, October 1989.

Hvorslev, M. J., 1951, *Time Lag and Soil Permeability in Ground-Water Observations*, Bull 36, U.S. Army Corps of Engineers, Waterways Station, Vicksburg, Mississippi.

Kaminsky, J. F., et al., 1993, *Remedial Investigation Final Report with Addenda for the Test Area North Groundwater Operable Unit 1-07B at the Idaho National Engineering Laboratory*, EGG-ER-10643, Rev. 0, August 1993.

Kuntz, M. A., et al., 1990, *Revised Geologic Map of the Idaho National Engineering Laboratory and Adjoining Areas, Eastern Idaho*, U.S. Geological Survey Open-file Report 90-333.

Kuntz, M. A., 1992, "A Model-Based Perspective of Basaltic Volcanism on the ESRP, Idaho," in: "Regional Geology of Eastern Idaho and Western Wyoming," *Geological Society of America Memoir 179*.

Leeman, W. P., 1982, "Olivine Tholeiitic Basalts of the Snake River Plain, Idaho," *Cenozoic Geology of Idaho*, Idaho Geological Survey Bulletin 26, pp. 181–191.

Lewis, B. D., and F. J. Goldstein, 1982, *Evaluation of a Predictive Ground-Water Solute-Transport Model at the Idaho National Engineering Laboratory*, IDO-22062, U.S. Geological Survey Water-Resources Investigation 82–25.

Lewis, B. D., and R. G. Jensen, 1984, *Hydrologic Conditions at the Idaho National Engineering Laboratory, Idaho: 1979-1981 Update*, U.S. Geological Survey Open-File Report 84-230, IDO-2066.

Mabey, D. R., 1982, *Geophysics and Tectonics of the Snake River Plain, Idaho*, Idaho Geological Survey Bulletin 26, pp. 139–154.

Mann, L. J., 1986, *Hydraulic Properties of Rock Units and Chemical Quality of Water for INEL-1; A 10,365-Foot Deep Test Hole Drilled at the Idaho National Engineering Laboratory, Idaho*, U.S. Geological Survey Water-Resources Investigations Report 86-4020, IDO-22070.

Moos, D., and C. A. Barton, 1990, *In-Situ Stress and Natural Fracturing at the INEL Site, Idaho*, Stanford University Department of Geophysics, EGG-NPR-10631, September.

Mundorff, M. J., E. G. Crosthwaite, and C. Kilburn, 1964, *Ground Water for Irrigation in the Snake River Basin in Idaho*, U.S. Geological Survey, Water Supply Paper 1654.

Nace, R. L., J. W. Stewart, W. C. Walton, et al., 1959, *Geography, Geology, and Water Resources of the National Reactor Testing Station, Idaho, Part 3. Hydrology and Water Resources*, U.S. Geological Survey, IDO-22034-USGS.

Nace, R. L., P. T. Voegeli, J. R. Jones, and M. Deutsch, 1975, *Generalized Geologic Framework of the National Reactor Testing Station, Idaho*, U.S. Geological Survey professional paper.

Pierce, K. L., and L. A. Morgan, 1992, "Track of the Yellowstone Hotspot: Volcanism, Faulting, and Uplift," *Geological Society of America Memoir 179*, pp. 1–53.

Pittman, J. R., R. G. Jensen, and P. R. Fischer, 1988, *Hydrologic Conditions at the Idaho National Engineering Laboratory, 1982 to 1985*, U.S. Geological Survey Water-Resources Investigations Report 89-4008.

Robertson, J. B., R. Schoen, and J. T. Barraclough, 1974, *The Influence of Liquid Waste Disposal on the Geochemistry of Water at the National Reactor Testing Station, Idaho: 1952–1970*, U.S. Geological Survey Open-File Report, IDO-22053, Waste Disposal and Processing TID-4500.

Sagendorf, J., 1991, *Meteorological Information for RWMC Flood Potential Studies*, U.S. Department of Commerce, National Oceanic and Atmospheric Administration, Environmental Research Laboratories, Air Resources Laboratory Field Research Division, Idaho Falls, Idaho.

Scott, W. E., 1982, "Surficial Geologic Map of the Eastern Snake River Plain and Adjacent Areas, Idaho and Wyoming," U.S. Geological Survey Miscellaneous Investigation Map I-1372.

Snake River Group of Malde, 1991, "Quaternary Geology and Structural History of the Snake River Plain, Idaho and Oregon," *The Geology of North America, K-2*, pp. 251–281.

van der Kamp, G., 1976, "Determining Aquifer Transmissivity by Means of Well Response Tests: The Underdamped Case," *Journal of Water Resources Research*, 12, 1, pp. 71–77.

Van Deusen, L., and R. Trout, 1990, *Draft, Phase I Remedial Investigation/Feasibility Study Work Plan and Addendums for the Warm Waste Pond Operable Unit at the Test Reactor Area of the Idaho National Engineering Laboratory (Volumes I and II)*, EGG-WM-8814, July 1990.

Van Haaften, D. H., K.N. Koslow, and C. J. Naretto, 1984, *Hydrologic Analysis of a Mackay Dam Failure During a Probable Maximum Flood on Big Lost River, Idaho*, SE-A-84-018, EG&G Idaho, Inc.

Whitehead, R. L., 1986, "Geohydrologic Framework of the Snake River Plain, Idaho and Western Oregon," *U.S. Geological Survey Atlas*, HA-681.

Wood, T. R., 1989, *Test Area North Pumping Tests*, EGG-ER-8438, January 1989.

Wood, T. R., L. C. Hull, and M. H. Doornbos, 1989, *Ground-Water Monitoring Plan and Interim Status Report for Central Facilities Landfill II*, EGG-ER-8496.